

Analyzing Materials Using Joint X-ray Fluorescence and Diffraction Spectra

Analyzing Materials Using Joint X-ray Fluorescence and Diffraction Spectra

By

Igor F. Mikhailov, Alexey A. Baturin
and Anton I. Mikhailov

Cambridge
Scholars
Publishing



Analyzing Materials Using Joint X-ray Fluorescence and Diffraction Spectra

By Igor F. Mikhailov, Alexey A. Baturin and Anton I. Mikhailov

This book first published 2020

Cambridge Scholars Publishing

Lady Stephenson Library, Newcastle upon Tyne, NE6 2PA, UK

British Library Cataloguing in Publication Data

A catalogue record for this book is available from the British Library

Copyright © 2020 by Igor F. Mikhailov, Alexey A. Baturin
and Anton I. Mikhailov

All rights for this book reserved. No part of this book may be reproduced, stored in a retrieval system, or transmitted, in any form or by any means, electronic, mechanical, photocopying, recording or otherwise, without the prior permission of the copyright owner.

ISBN (10): 1-5275-4246-7

ISBN (13): 978-1-5275-4246-4

CONTENTS

List of Legends	ix
Foreword	x
Chapter 1	1
Basic Principles Of X-Ray Analysis	
1.1 X-ray interaction with substance.....	1
1.2 Characteristics of X-ray spectra.....	5
1.3 Measuring the intensity of spectral lines.....	9
1.4 Wave-dispersion and energy-dispersion X-ray fluorescence analysis.....	11
1.5 General approaches for calculating X-ray spectra	15
1.6 Schemes for primary spectrum formation.....	20
1.7 Wave dispersion.....	27
1.7.1 Energy resolution and efficiency of a WDXRF spectrometer....	30
1.8 Dispersion by quantum energies and characteristics of solid state detectors for X-rays.....	32
1.8.1 Energy resolution and efficiency of solid-state detectors	34
1.8.2 Spectrum artifacts.....	37
1.8.3 Thickness of the detector active region	39
Conclusion to Chapter 1.....	42
Chapter 2	46
Wave-Dispersion X-Ray Fluorescence Analysis	
2.1 The main characteristics of traditional crystal-analyzers.....	46
2.2 Criterion for selecting materials of monochromators with a high reflectivity	48
2.3 The application of high-efficiency crystal-analyzers with low structure perfection; X-ray optic scheme with two Soller collimators.....	53
2.4 High-oriented pyrolytic graphite; reflection coefficient in different radiations	58
2.5 Monochromators based on fullerite C ₆₀ epitaxial films.....	60
2.5.1 Calculations of the structural factor in the rotation model ...	62
2.5.2 Ratio of reflection orders and determination of C ₆₀ molecule size	64

2.5.3 Dependence of the fullerite reflection coefficient on the wavelength in the range λ from 1.54 Å to 8.34 Å.....	70
2.5.4 Characteristics of spectra obtained with fullerite crystal analyzers.....	73
2.6 Multilayer X-ray mirrors.....	74
2.6.1 Structural characteristics	74
2.6.2 Short-period mirrors; dependence of the reflection coefficient on the operating wavelength range	81
2.6.3 Using long-period X-ray mirrors to measure light elements by fluorescence lines.....	84
Conclusion to Chapter 2.....	88
Chapter 3	89
Energy-Dispersion X-Ray Fluorescence Analysis	
3.1 Optimization of the primary beam formation unit.....	89
3.1.1 Conditions for optimizing the parameters of a primary radiation filter	89
3.1.2 Optimization of the secondary target parameters for the detection limit.....	96
3.1.3 Increasing the sensitivity of the scheme with a secondary target by filtrating the primary radiation.....	102
3.1.4 Multilayer secondary targets; optimization of layers by thickness and atomic number.....	109
3.1.5 Experimental study on the characteristics of a two-stage fluorescent lens.....	120
3.2 Quantitative X-ray phase analysis using secondary target fluorescence lines	126
3.2.1 Quantitative X-ray phase analysis of steel using ferrite and cementite Bragg reflections	127
3.2.2 Quantitative phase analysis of ferrite and cementite using an X-ray fluorescence spectrometer.....	132
3.2.3 Quantitative analysis using cementite reflections with a secondary target.....	134
Conclusion to Chapter 3.....	138

Chapter 4	139
Determination of Light Impurities Using the Compton and Rayleigh Scattering Intensity Ratio	
4.1 Theory	142
4.1.1 Introduction and restrictions.....	142
4.1.2 Scattering on a chaotic cluster of atoms	143
4.1.3 Scattering on molecules.....	146
4.1.4 Scattering by materials with an inhomogeneous distribution of impurities in depth	147
4.2 Specificity of measuring the incoherent scattering intensity	154
4.2.1 Using X-ray optical schemes to measure the scattering peaks	155
4.3 The possibilities of developed schemes for the determination of light elements using the ratio of the scattering peaks.....	158
4.4 Reducing the intensity of Bragg reflections due to the temperature factor	162
4.5 Displacement of the Compton band in scattering by bound electrons	170
Conclusion to Chapter 4.....	172
Chapter 5	174
Complex X-Ray Methods for the Analysis of Material Composition	
5.1 Determination of trace contaminants in pure materials.....	175
5.1.1 Express certification of material purity using the ratio of Compton and Rayleigh peak intensities	175
5.1.2 Determining the content of "trace" impurities in the light matrix.....	177
5.2 Studying the characteristics of thin films	181
5.3 Analyzing the distribution of impurities in the depth of the substrate.....	185
5.4 Determination of light elements in heterogeneous samples using WDXRF.....	193
5.5 Analyzing the composition of multiphase systems using combined X-ray scattering, fluorescence, and diffraction spectra	197
5.6 Experimental comparison of the analytical capabilities of various selective excitation schemes.....	202
5.7 Determination of the ash content in coal.....	207
5.7.1 Calibration plots	208
5.7.2 Experiment	212

5.8 Nano-impurities in objects of ecology, biology, and medicine ...	216
5.8.1 Rapid diagnostics of urinary iodine using a portable EDXRF spectrometer	216
5.8.2 Biological tissues.....	226
5.8.3 Drinking water and food.....	228
Conclusions.....	230
References	231

LIST OF LEGENDS

λ	Wavelength in Å (1 Å=10 ⁻¹⁰ m)
μ	Mass attenuation coefficient
σ	Mass scattering coefficient
φ	Angle of incidence
ψ	Exit angle
θ	Bragg diffraction angle
2β	Scattering angle
d	Interplanar spacing
ρ	Density
ω	Fluorescence yield
C	Concentration of a chemical element in the material
C_{min}	Limit of detection
E	Radiation energy
I	Radiation intensity
t	Thickness
Z	Atomic number of a chemical element
WDXRF	Wavelength Dispersion X-ray Fluorescence
EDXRF	Energy Dispersion X-ray Fluorescence

FOREWORD

Determination of the material composition using the XRF method is carried out by the intensity of fluorescent radiation, while the primary radiation, which is scattered by the sample, and the diffraction reflections are considered to be background signals and are rarely used for analytical purposes. To increase the sensitivity of the analysis, empirical methods are commonly used—filters, secondary emitters, monochromators, etc.—in the X-ray optical scheme. However, with the empirical approach, it is impossible to determine whether the adopted measurement scheme provides the highest sensitivity for the given chemical elements, or if there is another, more effective solution.

Apparently, in order to achieve the highest sensitivity of the analysis, it is necessary to optimally form the entire X-ray spectrum, including X-ray fluorescence, scattering (coherent and incoherent), and diffraction using a crystal lattice. In this book, we propose a general approach to solve the problem of optimizing X-ray optical schemes for the formation of spectra using the criterion of detection limit.

In recent years, a significant number of papers have appeared in which scattered radiation measurements have been used to correct XRF results. Even semi-quantitative measurements of coherent and incoherent (Compton) scatter peaks expand XRF capabilities in determining light elements. However, a precision measurement of the scattering peaks is

difficult to achieve in traditional XRF schemes. The optimization of X-ray optical schemes provides high accuracy when measuring scattered radiation. This opens up prospects for determining elements (up to hydrogen) with a small atomic number.

With the optimization of the X-ray optical schemes, conditions are created for reliably measuring the diffraction reflections of the material under study in the combined spectrum. The identification of these reflections allows one to carry out a quantitative phase analysis and to determine elements with a small atomic number by the amount of the phase that contains them (for example, carbon in cementite).

The specific conditions to measure the combined spectra, as well as the experimental X-ray optical schemes and their individual elements have been developed. Numerous examples on solving specific analytical problems are given: trace impurities at the level of 0.1–1.0 ppm; elements with a low atomic number from 6 (C) to 1 (H); phases based on light elements; and depth distribution of impurities in the bulk, etc.

The solution to the complex problem of forming a combined X-ray spectrum, including fluorescent, scattered, and diffracted radiation, gives an opportunity to expand the applications of X-ray methods when studying material composition, both in terms of the range of chemical elements and the sensitivity.

Over the past hundred years, many articles, monographs, and textbooks on X-ray analysis methods have been published. The authors hope that the reader is familiar with the fundamental works in this field and so they have,

therefore, limited themselves to mentioning the basic principles and literary references.

Acknowledgments

The main developments presented in the monograph are made at the Department of Physics of Metals and Semiconductors at the NTU "Kharkov Polytechnic Institute". The authors thank Professors V.V. Kondratenko, E.N. Zubarev, V.E. Puha, V.V. Belozarov, A.A. Mamalouy, and S.V. Malykhin for many years of cooperation and the provision of unique experimental results.

They are also thankful to employees of the X-ray Lab S.S. Borisova Ph.D. and L.P. Fomina Ph.D. for their continued support through their work, discussions, and helpful manuscript edits. The authors are especially grateful to the "Ukrrentgen" research and production firm (Kharkiv), headed by I.N. Babenko, and "Elvatekh" (Kiev), headed by A.S. Filippov, for their hardware support.

CHAPTER 1

BASIC PRINCIPLES OF X-RAY ANALYSIS

One of the basic methods for analyzing the composition of materials is X-ray fluorescence analysis (XRF). This method determines the positions and intensities of the lines in the spectrum of X-ray fluorescence that arise from the absorption of photons emitted by a primary source [1-4]. The interaction of the photons with a substance is not only limited by their absorption and emission of the fluorescence radiation. Also, an essential role is played by the phenomena of scattering atoms [2, 5] and diffraction reflection from the crystalline lattice of the material [6]. These phenomena are well studied and used for the structure certification of materials; however, in the framework of XRF, these were traditionally considered to be a background source. In the present work, we have shown that these phenomena can be used in combination with XRF to determine the chemical composition.

1.1 X-ray interaction with substance

X-ray radiation passing through a substance is attenuated according to the known Buger-Lambert-Baer law [2, 3]:

$$I = I_0 \exp(-\mu_l t) \quad (1.1)$$

where I_0 is the intensity of the primary radiation; I is the intensity of the radiation after passing through the layer with thickness, t ; and μ_l is the linear attenuation coefficient characterizing the attenuation of X-rays per unit path length.

Usually, the mass attenuation coefficient is used for these calculations: $\mu = \mu_l / \rho$, where ρ is the substance density. The attenuation is caused by two processes: absorption, τ , and scattering, σ [2, 4]. So that,

$$\mu = \tau + \sigma \quad (1.2)$$

When absorbed, a photon ionizes the atom's internal electron shells. The system tends to return to the most favorable energy state. This is accomplished by electron transfer from a more distant nucleus shell; for example, L , to an unoccupied inner level K (Fig. 1.1). Wherein the electron emits an energy portion equal to the difference between the energies of the shells. The wavelength of the emitted fluorescence radiation is characteristic for a certain element.

The probability of an electron transfer to the K -level that emits fluorescence radiation, ω_k , is called the fluorescence yield. This probability is reduced by the so-called Auger effect, which appears if a secondary radiation quantum is generated by an excited; for example, a K -shell interacting with electrons from more distant shells. As a result, the K -series radiation is absent outside of the atom; however, L - or M -series radiation and a free

Auger-electron are emitted. The probability of the Auger-electron emitting, a_k , is related with the fluorescence yield, ω_k , as

$$\omega_k + a_k = 1 \quad (1.3)$$

To evaluate the fluorescence yield, the following approximate formula is used [4]:

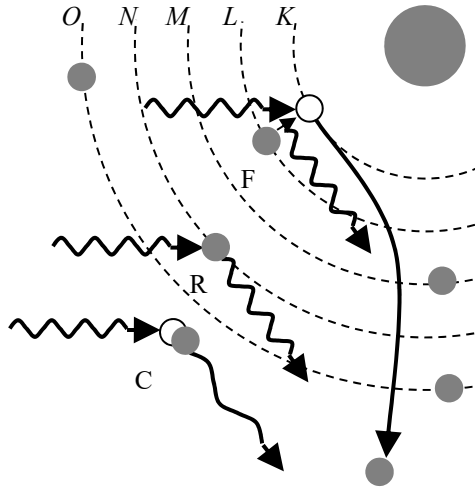


Figure 1.1: Processes accompanying the passage of X-rays through substance: F, the absorption of a photon and emitting fluorescence radiation; R, coherent (Rayleigh) scattering; C incoherent (Compton) scattering.

$$\omega_q = Z^4 / (a_q + Z^4) \quad (1.4)$$

where Z is the atomic number; q is the number of the level (the coefficients for K -, L -, and M - series: $a_K = 1,06 \cdot 10^6$; $a_L = 1 \cdot 10^8$; $a_M = 1,4 \cdot 10^9$).

The dependence of the absorption coefficient τ on the wavelength λ is a piecewise continuous function. The wavelengths corresponding to the excitation energies of K -, L_I -, L_{II} -, L_{III} -, M_I , and other atomic levels have absorption jumps, S_q . The relative portion of the photons absorbed by a q -level is $(S_q - 1)/S_q$. Between the absorption jumps, the function $\tau(\lambda)$ is approximated by the relation [4]:

$$\tau(\lambda) = G \lambda^\alpha Z^\beta, \quad (1.5)$$

where $\alpha \approx 2.7$; $\beta \approx 2.5 \div 3$; G is a tabular coefficient [9]. For practical calculations, one can use the appropriate tables.

The physical basis of the quantitative X-ray spectral analysis is Moseley's law, which establishes a single-valued relationship between the wavelengths λ of analytical lines and the atomic numbers Z of the corresponding chemical elements. In particular, for $K_{\alpha 1}$ -lines, this is written as [4]

$$\lambda = (Z - 1)^{-2} \times 1.21 \times 10^3, [\text{\AA}] \quad (1.6)$$

The scattering coefficient consists of two components: $\sigma = \sigma_R + \sigma_C$; σ_R is coherent (Rayleigh), and σ_C is incoherent (Compton).

Coherent scattering is caused by the elastic interaction of a photon with bound electrons of atomic shells, when the direction of the photon motion is changed but its energy remains the same. Under incoherent (Compton) scattering, a part of the energy is transferred to a loosely coupled electron, which results in increasing the wavelength of the scattered radiation (Fig. 1.1). The ratio of the coherent-to-incoherent scattering intensities is drasti-

cally changed as the atomic number of the material decreases. This effect causes a unique opportunity for the quantitative analysis of light elements, up to hydrogen, using X-ray methods. This opportunity was predicted by Compton [7] and will be discussed in Chapter 4.

The intensity of the scattered X-rays is about factor 100 lower than the absorbed beam intensity; this is caused by the ratio (σ/μ) of scattering (σ) and attenuation (μ) mass coefficients.

1.2 Characteristics of X-ray spectra

An X-ray spectrum is the dependence of signal intensity on the energy (wavelength) of an X-ray quantum (Fig. 1.2). In the X-ray spectra, both processes considered in the previous section are observed: absorption and scattering. The absorption is accompanied by the fluorescence characteristic emission of the sample material; therefore, the fluorescence atoms' analytical lines appear in the spectrum. In Figure 1.2, these are the lines with wavelengths more than 1 Å (Ni- K_β , Cu- K_α , etc.). The scattering manifests itself through two peaks: the coherent scattering of the characteristic radiation of the X-ray tube anode material (Ag- K_α in the figure), and the incoherent scattering (not shown in the figure). In addition, a broadband background exists, which is caused by the scattering of the bremsstrahlung radiation (continuous spectrum). Thus, the spectrum consists of analytical and background signals, which are different widths. The width of the analytical peak is determined by the physical width of the spectral line (about 1 eV) and the energy resolution of the X-ray spectrometer, which varies from 1 eV to 500 eV depending on the type of the spectrometer and the energy of quanta. *Spectral resolution* is the minimum revealed difference

between the energies of two neighboring lines; this is determined by their half-width and, consequently, by the characteristics of the spectrometer.

The quantitative analysis of the chemical composition is accomplished through the intensity of the analytical lines. The background signal has a smooth function with a characteristic decrement of ~ 1 keV. This broad-band background is superimposed on the fluorescence spectrum and complicates the ability to reveal the weak lines: i.e., it reduces the sensitivity of the analysis.

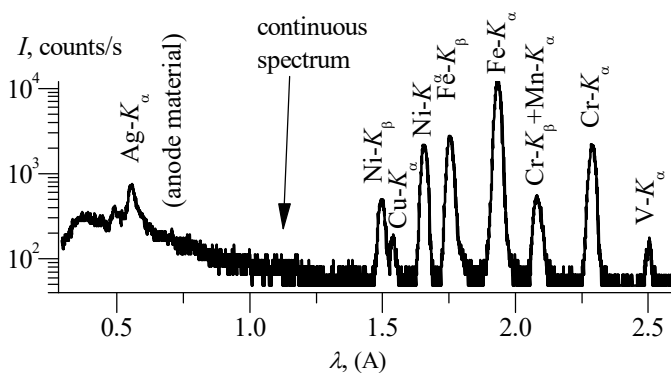


Figure 1.2: X-ray fluorescence spectrum of a steel standard sample

X-ray spectra are divided into the series labeled with the following letters: K , L , M , N , and O . Each series consists of lines labeled in order of the increasing radiation energy (α , β , γ , etc.) with digital indices: $K_{\alpha 1}$, $K_{\alpha 2}$, $K_{\beta 1}$, $K_{\beta 2}$, $L_{\alpha 1}$, $L_{\alpha 2}$, etc. The relative intensity of the line in the series is determined by the probability of the corresponding electron transfers between the levels. It is also characterized by the statistical weight p .

In comparison with optical ones, X-ray spectra are simple and consist of a small number of lines. This is caused by the fact that X-ray spectra are due to transfers to inner electron shells that have not been deformed by chemical bonds. The simplicity and stability of X-ray spectra under the formation of chemical bonds provides a unique opportunity to solve the inverse problem of determining the sample chemical composition using the full-profile analysis of its X-ray spectrum. The solution to the problem is impossible for optical spectra because of their significant variations for different phases; this fact does not allow for choosing a stable basis for the expansion of the functional.

One of the main spectral characteristics is *contrast*: the ratio of the analytical line peak intensity to the background under this line. Evidently, for the given integral intensity of the analytical line, the smaller its half-width, the higher its contrast. In this sense, the highest contrast is characteristic for lines with their half-width close to the *physical* width of lines: i.e. when the *apparatus* factor of line blurring is absent. Using this assumption, the theoretical detection limit for impurities for XRF was obtained in [8]. However, in real instruments, the contribution of this apparatus factor into the line blurring is high and will be discussed below.

Thus, the smaller the spectral line half-width, the higher the contrast and spectral resolution, or, in other words, the higher the spectrum quality. However, the high quality of the spectrum is not enough to provide a high sensitivity in the analysis. A characteristic of analysis sensitivity is the *detection limit*: the smallest concentration of the element revealed in the sample. According to the statistical interpretation, the detection limit, C_{\min} , is the content of the element in the sample, in which the average value of

the difference between the analytical signal I and the background signal I_b is a factor k larger than the standard deviation σ_b of the background signal [4, 9]. The value of k is determined by the chosen statistical certainty. At $k = 3$, which is more often used in practice, the statistical certainty of correct detection is 50%, and the false one is 14 %.

The *detection limit*, C_{\min} , is determined by the formula:

$$C_{\min} = 3 \frac{\sqrt{I_b}}{\partial I / \partial C} = \frac{3}{\sqrt{K \cdot \partial I / \partial C}}. \quad (1.7)$$

The variation of signal (pulse count) per 1 % of impurity content $\partial I / \partial C$

is called *concentration sensitivity* and $K = \frac{\partial I / \partial C}{I_b}$ is the signal contrast for an impurity with a concentration of 1 % mass. In order to lower the C_{\min} , along with contrast increasing, it is necessary to raise the concentration sensitivity (at the given X-ray tube power), which is determined by the *luminosity* of the spectrometer.

The *luminosity* of the spectrometer (ε) is the ratio of the emergent and incident radiation energies [10]. This ratio depends on the applied X-ray optic scheme and characteristics of its components (monochromators, secondary targets, detectors, etc.). Essentially, the *luminosity* ε is the device efficiency.

1.3 Measuring the intensity of spectral lines

The quantitative analysis of the chemical element content is carried out by the calibration function method [3]. According to this method, measuring the intensity of analytical lines is fulfilled for standards with certified concentrations of corresponding elements at the first stage. From the results of the measurements, a plot of the concentration versus the fluorescence integral intensity is built for each chemical element. Using this calibration function, the background value I_b is determined by extrapolation to the zero concentration, and the concentration sensitivity $\partial I/\partial C$ by the slope of the plot. The detection limit is calculated by Eq. (1.7) for a measuring time equal to that of I_b and $\partial I/\partial C$, and the standard deviation is determined by the scattering of experimental values relative to the regularization curve. At the second stage, fluorescence line intensities are measured for the test sample and then the calibration plot determines the concentration of the corresponding impurity. In the case of a significant difference between the base materials of the standard and the test samples, a correction using the base effect in the intensity of analytical line is carried out and the corresponding correction is entered into the concentration value.

The analytical line integral intensity of an impurity is measured in the specific energy range created by the spectrometer energy resolution. It is clear that the narrower the chosen range, the smaller the number of counts for the same measurement time. This would result in a predominant $\partial I/\partial C$ decrease in comparison with $\sqrt{I_b}$ in Eq. (1.7) and, consequently, to an increase in C_{\min} . However, an unreasonable expansion of the energy interval would lead to a decrease in contrast due to capturing the background.

Thus, it is intuitively clear that, in order to obtain the minimum C_{\min} , we should optimize the measurement interval for the impurity analytical line integral intensity.

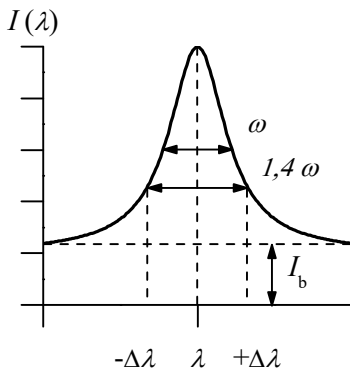


Figure 1.3: Optimal wavelength interval to measure intensity

We will now consider the measurement optimal interval problem in more detail. The shape of an analytical line is given by the quadratic Cauchy function [11] (Fig. 1.3):

$$I(\lambda) = I \left(1 + \frac{\lambda^2}{\omega/2} \right)^{-1} \quad (1.8)$$

where I is the peak intensity and ω is the line width at the half-maximum height.

Measurements of the integral intensity are carried out in the range of $\pm\Delta\lambda$ at $I_b = \text{const}$:

$$I(\text{int}) = \int_{-\Delta\lambda}^{\Delta\lambda} I \left(1 + \frac{\lambda^2}{\omega/2} \right)^{-1} d\lambda = I \omega \operatorname{arctg} \left(\frac{\Delta\lambda}{\omega/2} \right),$$

$$I_b(\text{int}) = I_b 2\Delta\lambda \quad (1.9)$$

Substituting (1.9) into (1.7) we obtain

$$C_{\min} = 3 \frac{\sqrt{I_b 2 \Delta\lambda}}{I \omega \operatorname{arctg} \left(\frac{\Delta\lambda}{\omega/2} \right)}. \quad (1.10)$$

By optimizing $\Delta\lambda$ from the condition of $\partial C_{\min}/\partial(\Delta\lambda) = 0$, we obtain the equation:

$$\operatorname{arctg} \left(\frac{\Delta\lambda}{\omega/2} \right) - \frac{\Delta\lambda \omega}{(\omega^2/4 + \Delta\lambda^2)} = 0. \quad (1.11)$$

The numerical decision of Eq. (1.11) gives the optimal interval for the integral intensity measurements, $2 \Delta\lambda = 1.4 \omega$, in which the minimum value of C_{\min} can be obtained. All subsequent experimental measurements of analytical line intensities in EDXRF were fulfilled in this energy range.

1.4 Wave-dispersion and energy-dispersion X-ray fluorescence analysis

Various X-ray schemes were applied to reduce the background signal and increasing the sensitivity of analysis [12, 13]. As previously stated, the main source of the background is the X-ray tube bremsstrahlung emission, which is scattered at the sample and spectrometer components, and also gets into the detector. Therefore, to prevent this signal from entering the

detector, the bremsstrahlung intensity should be drastically reduced directly after the X-ray tube or using filter collimation systems that are installed between the sample and the detector should protect it. Thus, we can select two basic nodes from an X-ray optic scheme: the primary spectrum formation unit and the spectrum registration unit. In general, the XRF scheme includes the following main nodes (Fig. 1.4): an X-ray tube, a primary spectrum formation unit, and a spectrum registration unit.

According to the distribution of functions between the primary spectrum formation unit and the registration unit, spectrometers are distinguished as either having wave-dispersion (WDXRF) or energy-dispersion (EDXRF).

We will distinguish between the broadband and selective excitation of the sample's fluorescence. The broadband excitation is caused by the bremsstrahlung radiation of the X-ray tube and always results in scattering backgrounds in X-ray spectra. The selective excitation is produced by a system of monochromatic lines obtained in the formation unit. With the selective excitation, the level of the broadband background is extremely low and created by the multiple scattering of the bremsstrahlung radiation. However, the selective excitation is always associated with a large loss of intensity and can only be applied in the devices with high luminosity.

The main functional difference between WDXRF and EDXRF spectrometers are as follows:

- WDXRF uses broadband fluorescence excitation from the sample and selective detection.
- EDXRF uses broadband or selective fluorescence excitation from the sample and broadband detection.

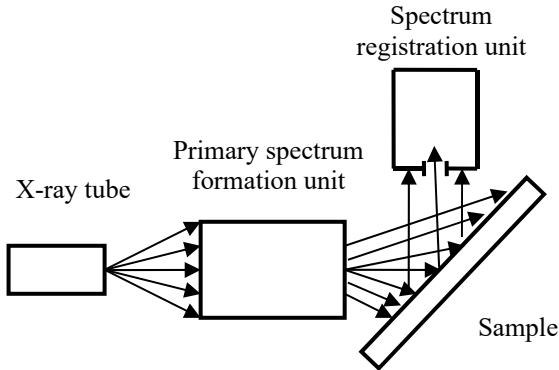


Figure 1.4: X-ray optic scheme for XRF

The broadband fluorescence excitation of the sample means that the primary spectrum formation unit is practically absent. In some cases, focusing capillary lenses are applied [5]. The X-ray tube radiation falls on the sample without any monochromatization. Unambiguously, this provides a high intensity of secondary emissions from the sample's chemical elements. However, getting into the registration unit, the sample radiation passes a long path through the collimation system and reflects from the crystal-analyzer, thus losing up to 99 % of its intensity. In order to prevent the absorption of the signal by air, the body of the WDXRF spectrometer is evacuated. Their comparably large dimensions and energy consumption characterize these types of spectrometers.

EDXRF spectrometers have high luminosity and can use both broadband and selective excitation of fluorescence. Under broadband excitation, the fluxes are so high that they exceed the permissible load of the detector and degrade the quality of spectra. Therefore, the X-ray tube power should be

limited and the measurements of the spectrum should be fulfilled in parts. However, the high level of the scattering background with broadband excitation is the principal limitation of the analysis' sensitivity. With the selective excitation, the sensitivity can be significantly increased using the calculation of the parameters for the formation unit (see Section 3).

EDXRF spectrometers use a broadband detection regime, where the detector simultaneously registers photons of all energies [13]. The detector is located a few millimeters away from the sample, thus providing a larger aperture for capturing the fluorescence radiation; this makes it possible avoid vacuuming for most analytical problems. Compact X-ray schemes with broadband detection formed the basis for creation of portable X-ray spectrometers with high luminosity.

The main factor influencing the fluorescence spectrum contrast (particularly with the broadband detection) is the fluorescence excitation method, which is realized by the spectrum formation unit. Five main methods of fluorescence excitation are known [2, 5, 13–17]. The higher contrast is required to solve a specific analytical problem; this means that more energy must be removed from the X-ray tube spectrum. Thus, the contrast is achieved at the expense of X-ray scheme luminosity losses. In order of decreasing luminosity and increasing contrast of the spectrum, the following methods of fluorescence excitation are used in known X-ray schemes:

1. An X-ray tube primary spectrum with filtration [13];
2. A quasi-monochromatic spectrum of the secondary target fluorescence emission [13, 14];

3. An X-ray primary spectrum monochromatized using a reflection from the face of a single crystal [5, 15];
4. Polarized primary radiation [16];
5. A “grazing” beam at the Brewster angle of the total external reflection [17].

The X-ray fluorescence excitation method is set by the *primary spectrum formation unit* (PSFU). Optimizing the PSFU parameters: namely, the supply voltage, filter and target parameters, and the scheme’s geometry—provide the best spectral contrast and the minimum detection limit.

1.5 A general approach for calculating X-ray spectra

Optimization of the parameters mentioned in 1.4 is realized theoretically from the condition that the total differential of the detection limit C_{\min} is zero:

$$dC_{\min}(U, \tau, \mu, \sigma, t, \varphi, \psi) = 0, \quad (1.12)$$

Here U is the supply voltage. The filter and target parameters are mass coefficients of absorption (τ), attenuation (μ), and scattering (σ); t is the filter thickness. φ is an incident angle, and ψ is an exit angle from the beam and these mark the geometry parameters of the scheme.

When solving this problem, three X-ray fluxes were considered. $\Phi_{01}(\lambda)$ is the primary radiation flux (spectrum); $\Phi_{02}(\lambda)$ is the radiation flux which is formed by the fluorescence excitation unit; and $\Phi_{03}(\lambda)$ is the flux getting into the detector. The X-ray tube flux $\Phi_{01}(\lambda)$ includes the anode characteristic emission and the bremsstrahlung radiation [4]:

$$\Phi_{01}(\lambda) = \Phi_c(\lambda) + \sum_i \delta(\lambda - \lambda_i) \Phi_{ch}(\lambda)$$

Here $\delta(\lambda - \lambda_i)$ is a delta-function.

The $\Phi_{02}(\lambda)$ flux is determined by the spectrum forming unit, and will be discussed in detail below. The $\Phi_{03}(\lambda)$ flux sets the detection limit $C_{\min}(\lambda)$ for the i -th element emitting the fluorescence radiation with a wavelength λ_i . Using [1, 10], it can be expressed as

$$\begin{aligned} \Phi_{03}(\lambda) = & \frac{S_S \sin \varphi}{4\pi r^2} \times \frac{\Phi_{02}(\lambda) \sigma_3(\lambda)}{\mu_3(\lambda) \left(\frac{1}{\sin \varphi} + \frac{1}{\sin \psi} \right)} + \frac{S_S \sin \varphi}{4\pi r^2} \times \\ & \times \sum_{i=1}^n \frac{1}{1 + \frac{(\lambda_i - \lambda)^2}{(\Delta\lambda_i/2)^2}} \frac{1}{\Delta\lambda_i} C_i p_i \omega_{qi} \left(1 - \frac{1}{S_{qi}} \right) \int_{\lambda_{ed}}^{\lambda_{qi}} \frac{\Phi_{02}(\lambda) \tau_i(\lambda)}{\mu_3(\lambda) + \mu_3(\lambda_i)} d\lambda \end{aligned} \quad (1.13)$$

where S_S is the sample irradiated area “seen” by the detector; r is the distance between the sample and the detector; λ_{ed} is the wavelength of the continuum spectrum edge; $\Delta\lambda_i$ is a half-width of the spectral line (spectrometer resolution); $\sigma_3(\lambda)$ and $\mu_3(\lambda)$ are, respectively, mass coefficients of scattering and attenuation of the $\Phi_{02}(\lambda)$ flux by the sample material; $\tau_i(\lambda)$ is the mass coefficient of the $\Phi_{02}(\lambda)$ flux absorption by atoms from the analyzed i -th chemical element; $\mu_3(\lambda_i)$ is the mass coefficient of the attenuation of the i -th chemical element fluorescence radiation by the sample material; C_i is the concentration of the analyzed i -th chemical element; p_i is the line relative intensity in the spectral series; and ω_{qi} is the fluorescence yield for the i -th chemical element.

The first summand in (1.13) describes the function of scattering the $\Phi_{02}(\lambda)$ flux and determines the main component of the background. The second summand describes the analytical lines of the sample chemical elements. The line profile is given by the Cauchy function. The optimization, which uses the criterion of C_{\min} , assumes the substitution of I_b (background) and the $\partial I_i / \partial C_i$ in (1.7). The contrast of the fluorescence spectrum or the “peak-to-background” ratio for the i -th element can be calculated as

$$K(\lambda) = C_i p_i \omega_{qi} \left(1 - \frac{1}{S_{qi}}\right) \frac{\sum_{i=1}^n \frac{1}{1 + \frac{(\lambda_i - \lambda)^2}{(\Delta\lambda_i/2)^2}} \frac{1}{\Delta\lambda_i} \int_{\lambda_{\text{ed}}}^{\lambda_{qi}} \frac{\Phi_{02}(\lambda) \tau_i(\lambda)}{\mu_3(\lambda) + \mu_3(\lambda_i)} d\lambda}{\frac{\Phi_{02}(\lambda) \sigma_3(\lambda)}{\mu_3(\lambda) \left(\frac{1}{\sin\varphi} + \frac{1}{\sin\psi}\right)}}. \quad (1.14)$$

The detection limit is determined according to (1.7)

$$C_{\min}(\lambda) = \frac{3\sqrt{\sin\varphi}}{C_i p_i \omega_{qi} \left(1 - \frac{1}{S_{qi}}\right) \sqrt{\frac{S}{4\pi r^2}}} \times \frac{\sqrt{\frac{\Phi_{02}(\lambda) \sigma_3(\lambda)}{\mu_3(\lambda) \left(\frac{1}{\sin\varphi} + \frac{1}{\sin\psi}\right)}}}{\sum_{i=1}^n \frac{1}{1 + \frac{(\lambda_i - \lambda)^2}{(\Delta\lambda_i/2)^2}} \frac{1}{\Delta\lambda_i} \int_{\lambda_{\text{ed}}}^{\lambda_{qi}} \frac{\Phi_{02}(\lambda) \tau_i(\lambda)}{\mu_3(\lambda) + \mu_3(\lambda_i)} d\lambda} \quad (1.15)$$

The Eq. (1.14) and (1.15) are general and can be applied to any function of the primary spectrum: for example, for the X-ray tube or synchrotron radiation. On the basis of Eq. (1.15), the optimization problem for C_{\min} can be considered in its general form, according to Eq. (1.12). In our monograph, all calculations of X-ray schemes for X-ray tube primary radiation were based on this approach.

The number of photons emitted per 1 s within the solid angle, which is 1 steradian for the given characteristic line, determines the characteristic radiation intensity I_{ch} of the anode material. The bremsstrahlung radiation or the continuous spectrum is determined by the spectral density $\partial I_c / \partial \lambda$: the number of photons (in the unit energy interval) emitted per second within a solid angle of 1 steradian. The values, I_{ch} and $\partial I_c / \partial \lambda$, set the form of the characteristic and the continuous spectra of the X-ray tube. They are determined using the following formulas from [10]:

$$I_{\text{ch}} = 5 \times 10^{14} i_a \frac{\gamma \omega_q p R}{Z_a} \left(\frac{\lambda_{1q}}{\lambda_{\text{cd}}} - 1 \right)^{1.67} \left[\frac{\text{photon}}{\text{s sr}} \right], \quad (1.16)$$

$$I_c = -109 \times 10^8 Z_a i_a \frac{1}{\lambda^2} \left(\frac{\lambda}{\lambda_{\text{kp}}} - 1 \right) \left[\frac{\text{photon}}{\text{s sr A}} \right], \quad (1.17)$$

where $R = \left(1 - \frac{7 Z_a - 80}{14 Z_a - 80} \right)$, Z_a is the atomic number of the anode material; i_a is the anode current; $\gamma = 3.8 \cdot 10^{-2}$ for the K -series and 0.11 for the L -series; ω_q is the fluorescence yield; p is the portion of intensity in the spectral series; λ_{1q} is the absorption jump wavelength of the X-ray tube anode